

17. D. Harman, *Ann. N.Y. Acad. Sci.* **717**, 1 (1994).
18. R. S. Sohal, R. Weindruch, *Science* **273**, 59 (1996).
19. S. S. Lee, G. Ruvkun, *Nature* **418**, 287 (2002).
20. P. L. Larsen, C. F. Clarke, *Science* **295**, 120 (2002).
21. B. Rogina, R. A. Reenan, S. P. Nilsen, S. L. Helfand, *Science* **290**, 2137 (2000).
22. R. J. McCarter, J. Palmer, *Am. J. Physiol.* **263**, E448 (1992).
23. E. J. Masoro, B. P. Yu, H. A. Bertrand, *Proc. Natl. Acad. Sci. U.S.A.* **79**, 4239 (1982).
24. C. Kenyon, J. Chang, E. Gensch, A. Rudner, R. Tabtiang, *Nature* **366**, 461 (1993).
25. C. A. Wolkow, K. D. Kimura, M. S. Lee, G. Ruvkun, *Science* **290**, 147 (2000).
26. K. D. Kimura, H. A. Tissenbaum, Y. Liu, G. Ruvkun, *Science* **277**, 942 (1997).
27. M. Tatar *et al.*, *Science* **292**, 107 (2001).
28. D. J. Clancy *et al.*, *Science* **292**, 104 (2001).
29. E. Wertheimer, S. P. Lu, P. F. Backeljauw, M. L. Davenport, S. I. Taylor, *Nature Genet.* **5**, 71 (1993).
30. A. Krook, L. Brueton, S. O'Rahilly, *Lancet* **342**, 277 (1993).
31. D. Accili *et al.*, *Nature Genet.* **12**, 106 (1996).
32. H. Kim *et al.*, *Diabetologia* **35**, 261 (1992).

33. S. I. Taylor, T. Kadowaki, H. Kadowaki, D. Accili, A. Cama, C. McKeon, *Diabetes Care* **13**, 257 (1990).
34. We thank A. Kahn and G. Ruvkun for valuable discussion; M. D. Michael for assistance establishing the line; K. C. Hayes, J. N. Winnay, S. E. Curtis, K. Chalkey, R. Quinn for animal care. Supported by NIH grants to C.R.K. (DK 30136) and to B.B.K. (DK 43051 and 56116), and by a grant of the Deutsche Gesellschaft der Naturforscher Leopoldina to M.B. (BMBF-LPD 9901/8-32).

9 September 2002; accepted 11 December 2002

Disruption of Transforming Growth Factor- β Signaling in ELF β -Spectrin-Deficient Mice

Yi Tang,¹ Varalakshmi Katuri,¹ Allan Dillner,¹ Bibhuti Mishra,^{1*} Chu-Xia Deng,^{2*} Lopa Mishra^{1,3,4*}

Disruption of the adaptor protein ELF, a β -spectrin, leads to disruption of transforming growth factor- β (TGF- β) signaling by Smad proteins in mice. *Elf*^{-/-} mice exhibit a phenotype similar to *smad2*^{+/-}/*smad3*^{+/-} mutant mice of midgestational death due to gastrointestinal, liver, neural, and heart defects. We show that TGF- β triggers phosphorylation and association of ELF with Smad3 and Smad4, followed by nuclear translocation. ELF deficiency results in mislocalization of Smad3 and Smad4 and loss of the TGF- β -dependent transcriptional response, which could be rescued by overexpression of the COOH-terminal region of ELF. This study reveals an unexpected molecular link between a major dynamic scaffolding protein and a key signaling pathway.

Transforming growth factor- β (TGF- β) signals are conveyed through serine-threonine kinase receptors at the cell surface to specific intracellular mediators, the Smad proteins (1). Activation of Smad proteins results in their translocation to the nucleus and subsequent activation of gene expression (2). Vertebrates possess at least nine Smad proteins (3–8), which fall into three functional classes: (i) receptor-activated Smads (R-Smads)—Smad1, Smad2, Smad3, Smad5, and Smad8; (ii) co-mediator Smads—Smad4 and Smad10; and (iii) inhibitory Smads—Smad6 and Smad7. Activity of R-Smads and Smad4 can be modulated by adaptor proteins in the cytosol such as filamin and Smad anchor for receptor activation (SARA). Because such adaptors can control Smad access to TGF- β receptors (T β RI and T β RII), which activate Smad at the cell surface membrane, they play

a critical role in facilitating TGF- β functions such as growth, differentiation, vascular remodeling, and cell fate specification (1–9).

Cytoskeletal proteins belonging to the β -spectrin family are thought to regulate signal transduction by functioning as adaptor molecules (10–12). When expression of the β -spectrin gene *elf* (embryonic liver fodrin) was blocked, liver formation was inhibited (13), and a phenotype similar to mice with compound haploinsufficiency at Smad2 and Smad3 loci was seen (14, 15). To assess a possible role in TGF- β signaling, we generated ELF-deficient mice by gene targeting (fig. S1, Fig. 1) (16). Homozygous mutant *elf*^{-/-} mice were not detected, indicating that the *elf* mutation is a recessive embryonic lethal. Abnormal or degenerating embryos were recovered between embryonic day 8.5 (E8.5) and E16.5. At E9.5, *elf*^{-/-} embryos were readily distinguished from their wild-type littermates by their smaller body and head size and lack of a branching network of vessels in the yolk sac (Fig. 1B). *Elf*^{-/-} embryos were severely distorted at E11.5, with growth retardation and multiple defects (Fig. 1, C to G). Cardiovascular defects included an absence of the normal trabeculated pattern of myocardial tissue with altered, thickened myocardial fibers. The myoblasts in the *elf*^{-/-} mutants were markedly hyperplastic with an absence of linear arrangement

of nuclei, resulting in a small ventricular lumen, and occlusion at the atrioventricular region (Fig. 1, E and F). Phenotypic similarities between *smad2*^{+/-}/*smad3*^{+/-} and *elf*^{-/-} embryos included abnormal anatomy of primary brain vesicles (Fig. 1D), craniofacial abnormalities, aberrant gut formation, severe hypoplasia of the liver, and distorted liver architecture. In the *elf*^{-/-} liver, hepatocytes were not always arranged in cords, and there were few early intrahepatic bile ducts (Fig. 1, E and I). Reduced expression of α -fetoprotein, a liver marker, in *elf*^{-/-} and *smad2*^{+/-}/*smad3*^{+/-} mutants indicates that, although hepatic lineage is established, further differentiation and growth may be arrested (Fig. 1I).

The phenotypic similarity between *smad2*^{+/-}/*smad3*^{+/-} and *elf*^{-/-} mutants suggested cross talk between ELF and the Smad gene family. Yolk sac blood vessel dilatation observed in some of the *elf*^{-/-} mutants is reminiscent of the T β RI, T β RII, activin receptor-like kinase-1 (ALK1), and Smad5 mutants, suggesting a role for ELF in TGF- β signaling (3, 17). Analysis of mouse embryonic fibroblasts (MEFs) derived from wild-type and *elf*^{-/-} mutants showed that the *elf*^{-/-} MEFs did not respond to TGF- β 1 stimulation, but they did respond to platelet-derived growth factor (PDGF) (Fig. 1H) (18, 19). This was confirmed by transient transfection experiments in which reporter constructs containing Smad binding sequences upstream of a luciferase gene were expressed in wild-type and *elf*^{-/-} MEFs (19, 20).

To determine whether ELF associates with Smad2, Smad3, and Smad4, we immunoprecipitated endogenous ELF from cell extracts prepared from wild-type MEFs and HepG2 (a human liver cell line) cells that had been treated with TGF- β 1 (16, 21). TGF- β 1 treatment stimulated ELF and Smad3 phosphorylation (Fig. 2; fig. S2, A and B). In all cells, specific antisera to ELF immunoprecipitated Smad3 and Smad4 proteins only in the presence of TGF- β 1 (Fig. 2; fig. S2C). No association occurred with Smad2 (Fig. 2; fig. S2C). In contrast, ELF associated with two known spectrin binding structural proteins, ankyrin B and tropomyosin, only in the absence of TGF- β 1 (Fig. 2). This suggests that, upon stim-

¹Laboratory of Developmental Biology, Department of Medicine, Georgetown University, Washington, DC 20007, USA. ²Genetics of Development and Disease Branch, National Institute of Diabetes and Digestive and Kidney Diseases, National Institutes of Health, Department of Health and Human Services, Bethesda, MD 20878, USA. ³Department of Veterans Affairs at Washington, DC 20422, USA. ⁴Fels Institute for Cancer Research and Molecular Biology, Temple University, Philadelphia, PA 19140, USA.

*To whom correspondence should be addressed. E-mail: lm229@georgetown.edu and lopamishra@yahoo.com

ulation with TGF- β 1, phosphorylation of ELF could induce a conformational change that reduces its affinity for ankyrin and tropomyosin and facilitates an association with Smad3 and Smad4 instead (10).

Confocal microscopy revealed that treatment of HepG2 cells and wild-type MEFs with TGF- β 1 resulted in colocalization of Smad3 with ELF at the cell surface membrane (Fig. 3A) (20) and translocation of Smad4 and ELF to the nucleus (Fig. 3C) (16). However, Smad2 did not colocalize with ELF (Fig. 3B). Interestingly, Smad3 and Smad4 were mislocalized in the *elf*^{-/-} mutants (Fig. 3D) (20). In wild-type embryonic liver (E11.5), Smad3 was expressed along the cell surface membrane (Fig. 3D). However, in the *elf*^{-/-} mutants, Smad3 was localized in the cytoplasm and in an irregular pattern along the entire cell surface membrane (Fig. 3D). Similarly, Smad4 was aberrantly localized in the nucleus and the cytoplasm (20). These data indicate that, in the absence of ELF, Smad3 and Smad4 are mislocalized, disrupting TGF- β signaling.

Expression of the COOH-terminal domain of ELF (*elf*-C) that includes the ankyrin binding region, active phosphorylation sites at serine residues, and a hinge region regulating oligomer formation (13, 16) rescued TGF- β signaling in the *elf*^{-/-} mutant fibroblasts, and Smad3 localization to the cell surface membrane resembled wild-type localization (Fig. 3D, arrow). Smad3 mislocalization in *elf*^{-/-} fibroblasts was not rescued by expression of Smad3 or of the NH₂-terminal domain of ELF (*elf*-N) (Fig. 3D). To confirm that TGF- β -induced transactivation of target genes requires ELF, we examined expression of *c-fos* after TGF- β 1 stimulation in wild-type and *elf*^{-/-} fibroblasts. As expected, *c-fos* mRNA expression in response to TGF- β was eliminated in the *elf*^{-/-} fibroblasts (Fig. 3, E and F). Only transfection of *elf*^{-/-} fibroblasts with *elf*-C and not *elf*-N or Smad3 resulted in TGF- β -induced transactivation of *c-fos* (Fig. 3, E and F). These data suggest that a functional ELF spectrin represents a key regulatory element for TGF- β signaling by Smad modulation.

Both β -spectrin and microtubule-associated protein-2 (MAP-2) are important for microtubule (MT) bundling (10). As MTs have been shown to modulate Smad signaling (9), we examined their distribution and function and found them to be unaltered in *elf*^{-/-} embryos, suggesting that microtubule modulation of Smad proteins may be less relevant and secondary to ELF spectrins (20).

Filamin and SARA function as adaptors in TGF- β receptor signaling (22–24). Filamins, actin polymerization proteins, form scaffolds for multiple signaling proteins including SAP kinases such as MKK-4, Rho, Ras small guanosine triphosphatases, Smad2, and Smad5.

Fig. 1. (A) Loss of ELF in *elf*^{-/-} mouse embryos by immunoblot analysis of E9.5 or E11.5 embryo lysates with peptide-specific polyclonal antibodies (VA1, VA2, ELFABD). **(B to G)** Phenotypic analysis of *elf*^{-/-} embryos. **(B)** E9.5 *Elf*^{-/-} embryos exhibit yolk sac defects. (Left) Wild type (arrows, blood vessels). (Right) *elf*^{-/-}. **(C)** E11.5 embryos. Note the smaller liver and heart of *elf*^{-/-} embryos (right). **(D)** Hematoxylin and eosin (H&E)-stained sections of E11.5 embryos with forebrain defects. **(E)** H&E sections of E11.5 embryos reveal liver (L) and heart (H) defects in *elf*^{-/-} (right). **(F)** High-power view of H&E sections of heart in *elf*^{-/-} embryos exhibits abnormal myocardial tissue (right). **(G)** High-power view of H&E sections of gut (G) with flattened cells in *elf*^{-/-} (right) (arrows). **(H)** Thymidine incorporation studies. *Elf*^{-/-} MEFs do not respond to TGF- β , in contrast to PDGF. Dark blue bar, control without treatment; yellow bar, treatment with TGF- β 1; green bar, treatment with PDGF. Data were analyzed by paired *t*-test (*N* = 10). Significant differences are indicated: *, *P* < 0.001, compared with control. **(I)** Reduced expression of liver marker in *elf*^{-/-} embryos. Paraffin sections of embryos (E11.5) from wild type (left) and *elf*^{-/-} (right) were immunostained with antibody to α -fetoprotein (brown), labeling hepatocytes, in cords in wild-type liver (left) (arrows) and small clusters in *elf*^{-/-} (right) (arrows). He, hepatocytes.

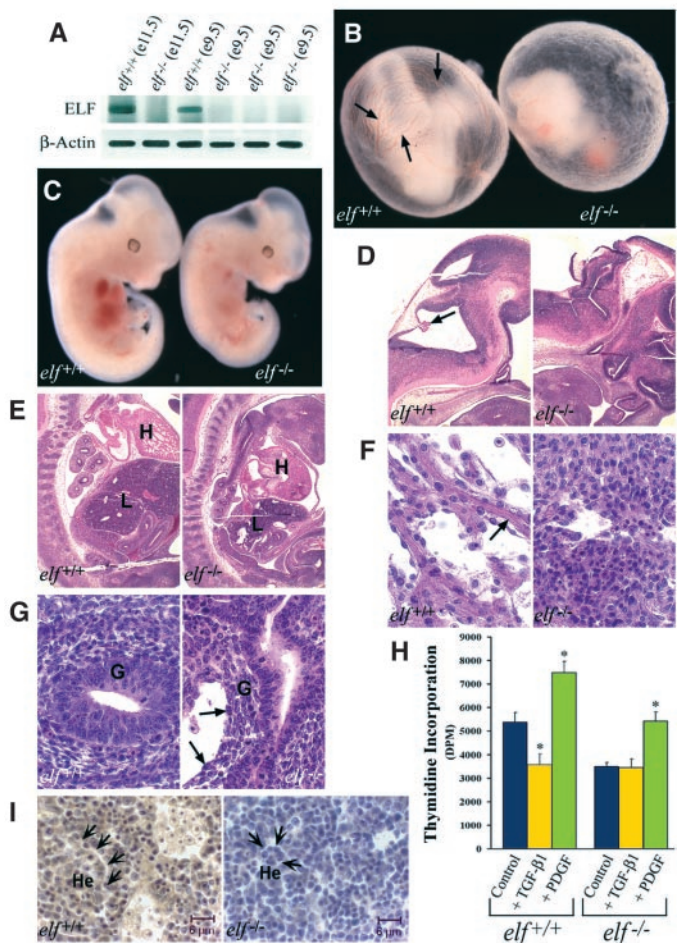


Fig. 2. Interaction of endogenous ELF and Smads in mammalian cells. Lysates from HepG2 cells were cultured with or without TGF- β 1 for 2 min (ELF phosphorylation) or 1 hour (the rest). They were then subjected to immunoprecipitation (IP) with preimmune sera and antibody to ELF and then immunoblotted (IB) with monoclonal or polyclonal antibody to Smad2, -3, -4, ankyrin B, and tropomyosin or subjected to immunoprecipitation with the monoclonal and polyclonal antibodies and then immunoblotted with antibody to ELF. Coprecipitation of Smad3/ELF, Smad3-Smad3, or Smad3-Smad4 is demonstrated (lane 8). TGF- β treatment induces phosphorylation of ELF (lane 10), Smad3 (58 kD) (lane 8), and Smad2 (58 kD) (lane 7), but not Smad4 (lane 9). In the presence of TGF- β 1, ELF interacts with Smad4 (60 kD) (lane 9). Coimmunoprecipitation of ELF with Smad3 and Smad4 is shown in the presence of TGF- β 1 (lane 10).

	1	2	3	4	5	6	7	8	9	10	11	12
TGF- β 1	-	-	-	-	-	-	+	+	+	+	+	+
IP: anti-ELF	-	-	-	+	-	-	-	-	+	-	-	-
IP: anti-T β R1	-	-	-	-	+	-	-	-	-	-	+	-
IP: anti-Smad3	-	-	+	-	-	-	-	+	-	-	-	-
IP: anti-Smad4	-	-	-	+	-	-	-	-	+	-	-	-
IP: anti-Smad2	+	-	-	-	-	-	+	-	-	-	-	-
IP: Preimmune	-	-	-	-	-	+	-	-	-	-	-	+
IB: anti-ELF												
IB: anti-T β R1												
IB: anti-Smad3												
IB: anti-Smad4												
IB: anti-Smad2												
IB: anti-Phosphoserine												
IB: anti-Ankyrin												
IB: anti-Tropomyosin												

REPORTS

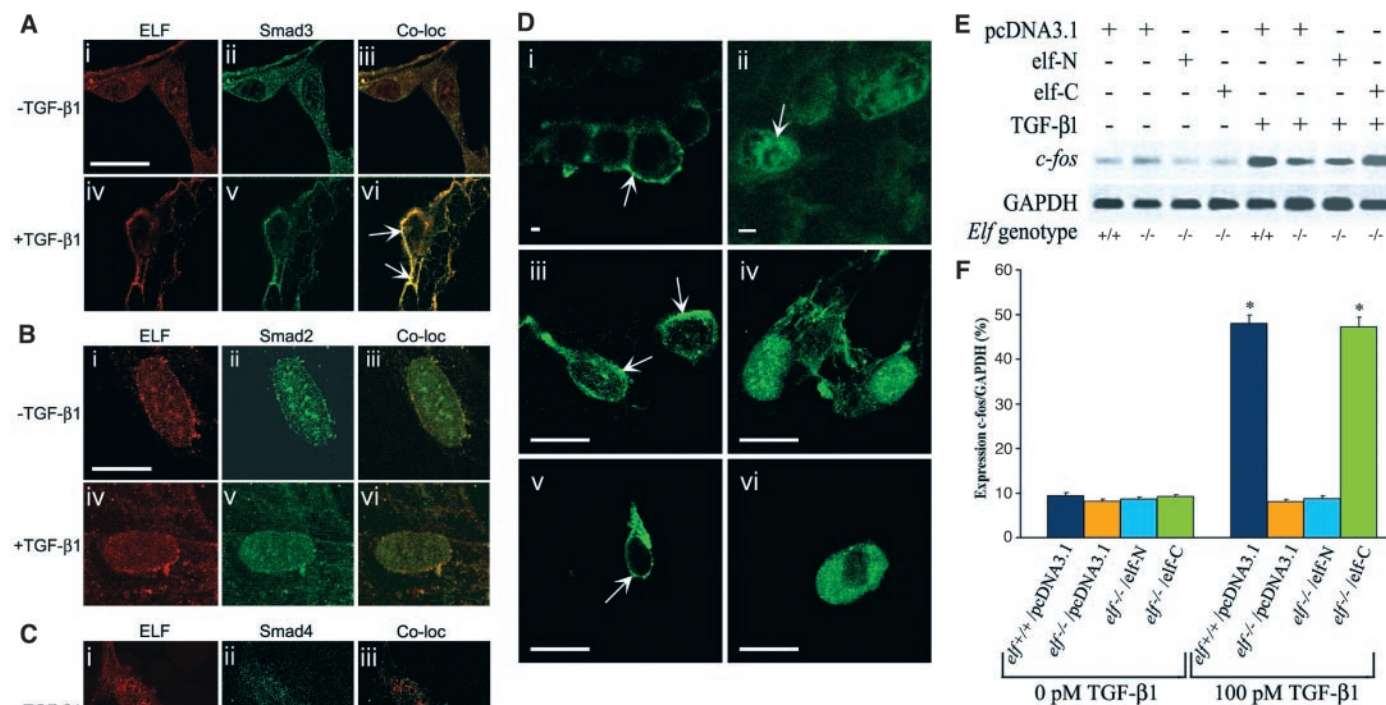


Fig. 3. (A to C) Colocalization of ELF and Smad2, -3, and -4 in TGF-β signaling. HepG2 cells were cultured with TGF-β1 for 1 hour followed by protein subcellular colocalization visualized by confocal microscopy. ELF localization is shown with ELF antibody and rhodamine-conjugated goat immunoglobulin G (IgG) to rabbit (red), whereas Smad2, -3, or -4 is seen with appropriate monoclonal antibodies and fluorescein isothiocyanate (FITC)-conjugated goat IgG to mouse (green). Colocalization of ELF and Smad3 and Smad4 appears as yellow. In (A to C), (i to iii) shows colocalization without TGF-β1 treatment; (iv to vi) shows colocalization with TGF-β1; (iii) and (vi) are overlays. Colocalization of ELF and Smad3 with TGF-β1 treatment for 1 hour appears as yellow spots in (A, vi) (arrows), and ELF

and Smad4 colocalization after TGF-β treatment appears as yellow spots in (C, vi) (arrow). Scale bars in (A to C) are 15 μm. **(D to F)** Rescue of Smad3 expression and TGF-β signaling in *elf*^{-/-} MEFs. (D, i) Immunofluorescent confocal microscopy showing normal Smad3 distribution (FITC) in E11.5 wild-type liver tissue (arrow). Scale bar, 1 μm. (D, ii) Smad3 distribution is abnormal in E11.5 *elf*^{-/-} liver (arrow). Bar = 1 μm. (D, iii to vi) Smad3 localization after treatment with TGF-β1. (D, iii) Smad3 expression in wild-type MEFs (arrows) transfected with pcDNA3.1 DNA only. (D, v) Transfection with ELF COOH-terminal region rescues Smad3 localization (arrow) compared with vector-transfected *elf*^{-/-} MEFs (D, iv), and transfection with ELF NH₂-terminal region (D, vi). Scale bars in (D, iii to vi) are 15 μm. **(E)** Absence of ELF impaired *c-fos* activation by TGF-β. Reconstitution of ELF expression restored TGF-β-mediated activation of *c-fos* with transfection with the ELF COOH-terminal region. GAPDH, glyceraldehyde phosphate dehydrogenase. **(F)** Quantitative analysis of normalized mRNA expression of *c-fos* in MEFs is shown in the bar graph. Dark blue bar, wild-type MEFs transfected with pcDNA3.1 DNA only; orange bar, *elf*^{-/-} MEFs transfected with pcDNA3.1 DNA only; light blue bar, *elf*^{-/-} MEFs transfected with cDNA encoding NH₂ terminus of ELF; green bar, *elf*^{-/-} MEFs transfected with cDNA encoding the COOH-terminal region of ELF. Representative exposures from five independent experiments are shown. Data were analyzed by analysis of variance followed by the Bonferroni *t*-test (*N* = 5). Significant differences are indicated: **P* < 0.01.

SARA, a major FYVE domain protein (named after the first letters of the four proteins containing it: Fab1p, YOTB, Vac1p, and EEA1), regulates the subcellular localization of unactivated R-Smads, potentially scaffolding the TGF-β receptor kinase to the Smad2 substrate (1, 2, 23). Analysis of SARA and filamin expression in liver revealed similar localization in the wild-type and *elf*^{-/-} embryos (20). Furthermore, SARA and filamin did not coimmunoprecipitate with ELF (fig. S2, D and E). We also examined whether ELF also associates with Smad1 and Smad5. Smad1 and Smad5 expression and localization were similar in wild-type and *elf*^{-/-} embryos (20) (fig. S3). ELF did not coimmunoprecipitate with either Smad1 or Smad5 from HepG2 cell extracts (fig. S2, D and E). As SARA, filamin, Smad1, and Smad5 do not appear to interact with ELF and are expressed equally in wild-type and *elf*^{-/-}

tissues, the R-Smads such as Smad3 and Smad4 may thus function through a different mechanism with ELF interactions, and this is supported by other studies pointing to different models of oligomerization (23, 24).

Taken together, these results point to ELF as an essential adaptor protein required for key events in the propagation of TGF-β signaling. We present evidence that, after stimulation with TGF-β, phosphorylated ELF may normally associate with endogenous receptor-associated Smad3, potentially facilitating its specific subcellular localization and activation by TβRI. Initially, ELF appears to associate with Smad3 and the TGF-β receptor complex. This interaction is followed by its interaction with Smad4, leading to their translocation to the nucleus. ELF, as a mediator of TGF-β signaling, appears to be independent of microtubule, SARA, or filamin modulation of Smad function, suggest-

ing a specificity for the regulatory role of ELF in TGF-β signaling. We speculate that the positive regulatory element by ELF could control the rate of Smad3 association and phosphorylation by activated TβRI as well as the translocation of phosphorylated Smads to the nucleus. These results provide new and unexpected insights into both TGF-β signaling and an essential role for the adaptor proteins of the β-spectrin family in this signaling process.

References and Notes

1. A. Moustakas, S. Souchelnytskyi, C.-H. Heldin, *J. Cell Sci.* **114**, 4359 (2001).
2. J. L. Wrana, L. Attisano, *Cytokine Growth Factor Rev.* **11**, 5 (2000).
3. M. J. Goumans, C. Mummery, *Int. J. Dev. Biol.* **44**, 253 (2000).
4. M. E. Engel, P. K. Datta, H. L. Moses, *J. Cell Biochem. Suppl.* **31**, 111 (1998).
5. M. Weinstein et al., *Proc. Natl. Acad. Sci. U.S.A.* **95**, 9378 (1998).

6. X. Yang *et al.*, *EMBO J.* **18**, 1280 (1999).
7. Y. Zhu *et al.*, *Cell* **94**, 703 (1998).
8. R. Derynck, R. J. Akhurst, A. Balmain, *Nature Genet.* **29**, 117 (2001).
9. C. Dong *et al.*, *Mol. Cell* **5**, 27 (2000).
10. V. Bennett, A. J. Baines, *Physiol. Rev.* **81**, 1353 (2001).
11. W. J. Nelson, P. J. Veshnock, *J. Cell Biol.* **103**, 1751 (1986).
12. M. A. De Matteis, J. S. Morrow, *J. Cell Sci.* **113**, 2331 (2000).
13. L. Mishra *et al.*, *Oncogene* **18**, 353 (1999).
14. M. Weinstein *et al.*, *Mol. Cell Biol.* **21**, 5122 (2001).
15. L. Mishra *et al.*, *Int. J. Dev. Biol.* **42**, 221 (1998).
16. Materials and methods are available as supporting material on Science Online.
17. J. Larsson *et al.*, *EMBO J.* **20**, 1663 (2001).
18. E. Piek *et al.*, *J. Cell Sci.* **112**, 4557 (1999).
19. E. Piek *et al.*, *J. Biol. Chem.* **276**, 19945 (2001).
20. Y. Tang *et al.*, data not shown.
21. C. D. Bhanumathy *et al.*, *Dev. Dyn.* **223**, 59 (2002).
22. A. Sasaki *et al.*, *J. Biol. Chem.* **276**, 17871 (2001).
23. A. Moustakas, C.-H. Heldin, *Genes Dev.* **16**, 1867 (2002).
24. L. Jayaram, J. Massague, *J. Biol. Chem.* **275**, 40710 (2000).
25. We thank C. Li for invaluable assistance with generating mutant *elf* mice and mouse blastocyte injection; S. J. Kim, A. Roberts, J. Wrana, L. Attisano, J. Massague, and A. Hata for the kind gift of Smad expression vectors; S. Danovitch, E. P. Reddy, and M. Zaslloff for their constructive criticism during the evolution of this manuscript; and R. Redman, E.

Fiores, A. Lorman, and E. Mishra for assistance with immunohistochemistry. Supported by NIH R01 DK56111 (L.M.), NIH R01 DK58637 (B.M.), a Veterans Administration merit award (L.M.), NIH R03 DK53861 (L.M.), the Betty and Harry Myerberg Foundation, and the Elisabeth and John Cox Foundation. This manuscript is dedicated to J.B.

Supporting Online Material

www.sciencemag.org/cgi/content/full/299/5606/574/DC1
Materials and Methods
Figs. S1 to S3
References

10 July 2002; accepted 6 December 2002

Dynamics of the Hippocampus During Encoding and Retrieval of Face-Name Pairs

Michael M. Zeineh,^{1,2} Stephen A. Engel,³ Paul M. Thompson,⁴ Susan Y. Bookheimer^{1,5*}

The medial temporal lobe (MTL) is critical in forming new memories, but how subregions within the MTL carry out encoding and retrieval processes in humans is unknown. Using new high-resolution functional magnetic resonance imaging (fMRI) acquisition and analysis methods, we identified mnemonic properties of different subregions within the hippocampal circuitry as human subjects learned to associate names with faces. The cornu ammonis (CA) fields 2 and 3 and the dentate gyrus were active relative to baseline only during encoding, and this activity decreased as associations were learned. Activity in the subiculum showed the same temporal decline, but primarily during retrieval. Our results demonstrate that subdivisions within the hippocampus make distinct contributions to new memory formation.

Structures within the MTL play a crucial role in forming new associations or episodic memories. Memory formation is a dynamic process: As new information becomes better learned, the hippocampus appears to be less critical (1, 2). The complex architecture of the hippocampus would seem to orchestrate this transition (3). Several studies have demonstrated some degree of subregion specificity within the hippocampus and related structures. In particular, recognition memory may require the perirhinal cortex (4), spatial memory may depend on the parahippocampal cortex (5, 6), and encoding and retrieval may involve the anterior and posterior hippocampus, respectively (7, 8). However, no studies to date have directly examined

how activity patterns within different substructures of the MTL change during learning. Here, we use functional magnetic resonance imaging (fMRI) in human volunteers to identify changes in the blood oxygen level–dependent (BOLD) response, reflecting neural activity, within different substructures of the MTL, as subjects progressively learn new associations.

Imaging the medial temporal subregions is technically challenging: Not only are the individual structures quite small, but the hippocampus itself is rolled into a compact spiral, making it difficult to isolate activity within any one region on the planar sections acquired in MRI scans. In order to parcel out neural activity in the subregions, we developed techniques to acquire high-resolution structural (0.4 by 0.4 mm) and functional (1.6 by 1.6 mm) MRI data and to localize functional activity precisely within the substructures of the hippocampus by “unfolding” the hippocampal cortex, revealing the entirety of each hippocampal subregion [CA fields 1, 2, and 3; dentate gyrus (DG); and subiculum] and adjacent neocortical regions (parahippocampal, entorhinal, perirhinal, and fusiform) in a single plane, or “flat map” (9–11) (Fig. 1). Briefly, this procedure begins by

first demarcating the boundaries between the architectonic subregions on the high-resolution structural MR images (Fig. 1A) and then segmenting and separating out the white matter and CSF throughout the MTL, retaining only the gray matter sheath (Fig. 1B). We then computationally extract and flatten the gray matter volume (similar to flattening the globe into a flat map of the world) and project the demarcated boundaries to produce unfolded flattened maps of the hippocampus (Fig. 1C). Because subjects vary in the anatomy of their MTLs, we constructed a template representing the typical anatomy of our subject population by averaging together the individual demarcation boundaries across subjects (12). Computational warping techniques transform an individual subject’s hippocampal maps to the flat hippocampal template space (13). The same transformation parameters are then applied to the coregistered functional MRI scans, which delivers high-resolution fMRI data in a standardized flat space. This procedure enabled us to measure activity over time in each subregion (e.g., the combined CA 2, 3, and DG termed “CA2,3DG,” CA 1, subiculum, fusiform, etc.) and to perform powerful group statistics across subjects.

Using this method, we scanned ten subjects while they performed a face-name association task in which a series of unfamiliar faces were paired with names (11). Learning the names of new faces is an essential aspect of everyday human memory that is known to engage the hippocampus (14, 15). We separated encoding blocks, where subjects saw the faces with the names and tried to commit them to memory, from recall blocks, where subjects saw the faces only and had to generate the correct name (Fig. 2). A distraction task prevented rote rehearsal between encoding and recall blocks. Subjects viewed the same face-name combinations four times so that the information was well learned by the last trial.

The subjects exhibited a positive learning curve over time as displayed in Fig. 3B. To determine the amount of new information successfully encoded on a given trial, we

¹Ahmanson-Lovelace Brain Mapping Center, UCLA School of Medicine, 660 Charles Young Drive South, Los Angeles, CA 90095–7085, USA. ²Medical Scientist Training Program, UCLA School of Medicine, ³UCLA Department of Psychology, Franz Hall, 1282a, Los Angeles, CA 90095–1563, USA. ⁴Laboratory of Neuroimaging, Department of Neurology, and ⁵UCLA Department of Psychiatry and Biobehavioral Sciences, UCLA School of Medicine, Los Angeles, CA 90095–1769, USA.

*To whom correspondence should be addressed. E-mail: sbook@ucla.edu